Acta Astronautica 184 (2021) 46–58

Contents lists available at ScienceDirect

Acta Astronautica

journal homepage: www.elsevier.com/locate/actaastro

Research Paper

Overview and analysis of the experimentally measured throat heat transfer in liquid rocket engine thrust chambers

Marco Pizzarelli *

Italian Space Agency, Italy

ARTICLE INFO

Keywords:
Liquid rocket engines
Hot-gas side heat transfer
Calorimeter and heat-sink thrust chambers
Heat transfer correlations

ABSTRACT

The design of high-performance liquid rocket engines is highly dependent on the management of the heat transfer rate produced by the combustion-gas and entering the thrust chamber wall. In particular, the life of the thrust chamber is mainly limited by the level of temperature and heat flux reached in the most thermally solicited part, which is the throat region. Consequently, experimental data of the hot-gas side heat transfer have been acquired since the 1950s. Such studies have increased over time in order to investigate the effect of different propellant combinations, propellant injector configurations, thrust chamber geometries, and combustion chamber pressures. In the present study, about 500 experimental heat transfer data taken from the open literature and relevant to the throat region are collected, manipulated, and analyzed with the main aim to find simplified rules to evaluate the peak heat transfer. Due to the intrinsic variability of the hot-gas side heat transfer and to the non-negligible measurement errors, the found correlations fit the whole set of experimental data with an uncertainty of up to 60%. However, considering specific propellant combinations, like oxygen–hydrogen or oxygen–hydrocarbons, far more reliable regressions are found.

1. Introduction

The hot-gas[1] generated and accelerated in a bi-propellant rocket engine thrust chamber creates an extremely harsh environment that represents one of the major design constraints of liquid rocket engines with high performances, that is, with maximized specific impulse for the selected onboard propellant. In fact, even if the thrust chamber is actively cooled, its life is mainly limited by the level of wall temperature and heat flux reached in the most thermally solicited part, which is the throat region. Consequently, the design of a thrust chamber is mainly a thermo-mechanical problem that can be assessed only with a proper characterization of the hot-gas side heat transfer. Such characterization, especially if not limited to the throat region, is also an essential input for the evaluation of important engine parameters like coolant pressure drop and temperature gain within the cooling system. Not by chance, one of the first steps in the development of a new rocket engine thrust chamber is often a series of heat-transfer experiments having the aim to measure the distribution of the heat transfer rate produced by the hot-gas. In such an early development phase, properly instrumented thrust chambers, often at a reduced scale in terms of geometry and combustion chamber pressure, are effective tools for evaluating the hot-gas side heat transfer and, possibly, comparing the effect of different injectors and thrust chamber designs. Fig. 1 presents a sketch of the inner contour of a thrust chamber indicating the main geometric design parameters that can have an impact on heat transfer, especially in the throat region.

The study of the hot-gas side heat transfer in liquid rocket engine thrust chambers began from the earliest stages of modern rocket development [1,2]. In particular, many experimental campaigns not explicitly related to any specific engine development have been carried out since the 1950s. The purpose of these campaigns was to identify and understand the main physical phenomena that drive the heat transfer from the hot-gas to the wall. It is worth mentioning the basic experiments made by Back (e.g., [3]) and Boldman (e.g., [4]) and their co-workers. They adopted simplified set-ups that permitted to focus on the pure convective heat transfer of a uniform hot-gas flow expanding in a convergent–divergent nozzle and free of effects like propellant injection and combustion, non-uniform propellant mixing, combustion "noise" (i.e., pressure oscillation with amplitudes of some percent of the mean pressure), large-scale secondary flows, chemical recombination of dissociated hot-gas species both in the free stream and in the boundary layer, and hot-gas radiation. These effects, which are mainly dependent on the propellant characteristics and the injector type and pattern, and

* Correspondence to: Agenzia Spaziale Italiana - Via del Politecnico snc, 00133 Roma, Italy.
E-mail address: marco.pizzarelli@asi.it.

[1] The term "hot-gas" refers to the propellant combustion products which, in general, may contain small fractions of condensed species both in liquid and solid phase.

https://doi.org/10.1016/j.actaastro.2021.03.028
Received 7 December 2020; Received in revised form 11 March 2021; Accepted 29 March 2021
Available online 9 April 2021

Nomenclature

A	thrust chamber cross-section area, [m^2]
C	coefficient of the heat transfer correlation, [-]
c_p	specific heat at constant pressure, [J/kg/K]
$c*$	characteristic velocity, [m/s]
D	thrust chamber cross-section diameter, [m]
$h_{g,T}$	temperature-based hot-gas side heat transfer coefficient, [$W/m^2/K$]
$h_{g,i}$	enthalpy-based hot-gas side heat transfer coefficient, [$kg/m^2/s$]
i	specific enthalpy, [J/kg]
k	thermal conductivity, [W/m/K]
L	length, [m]
L^*	characteristic length, [m]
Nu	$\frac{h_{g,T}D}{k}$, Nusselt number, [-]
o/f	oxidizer-to-fuel mass mixture ratio, [-]
p	pressure, [Pa]
Pr	$\frac{\mu c_p}{k}$, Prandtl number, [-]
q	heat flux, [W/m^2]
Re	$\frac{\rho u D}{\mu}$, Reynolds number, [-]
R_c	thrust chamber radius of curvature upstream the throat, [m]
St	$\frac{h_{g,i}}{\rho u}$, Stanton number, [-]
T	temperature, [K]
u	velocity, [m/s]
V_c	thrust chamber volume from the injector plate to the throat section, [m^3]
ε_c	contraction ratio, [-]
η_{c*}	combustion efficiency, [-]
θ_c	convergent angle, [rad]
μ	viscosity, [Pa s]
ρ	density, [kg/m^3]

Subscripts

aw	adiabatic wall
con	convergent section
cyl	cylinder section
e	chemical equilibrium composition in the boundary layer
f	frozen chemical composition in the boundary layer
fit	fit value
id	ideal combustion
t	throat section
w	hot-gas side wall
0	combustion chamber
∞	free-stream
$+2\sigma$	value including 95.45% of the data

that may profoundly influence the heat transfer in the subsonic portion of the thrust chambers, were intentionally discarded by using mildly heated and compressed air and large calming sections. In addition to looking into the basic phenomena, these seminal studies have made it possible to obtain correlations for the convective heat transfer coefficient which are easy to use as design tools and are still in use today. The most adopted one was introduced by Bartz [5]. However, because the hot-gas side heat transfer in a real rocket engine is sensitive to the used propellant, the injection scheme and pressure, and the thrust chamber

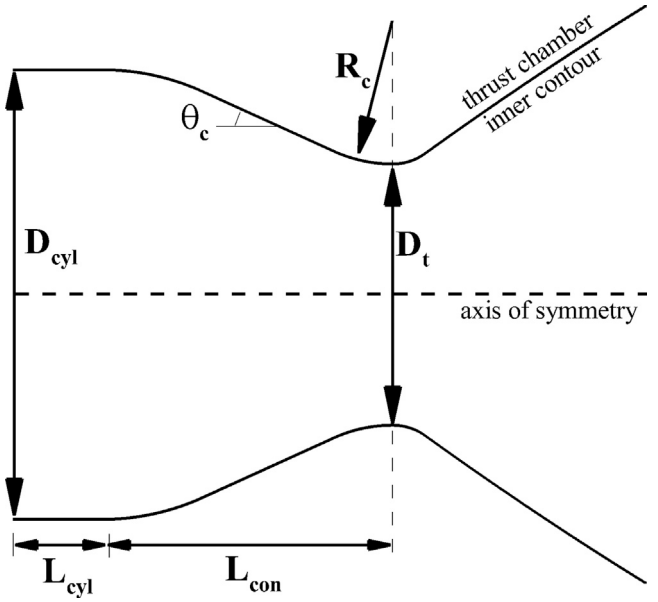

Fig. 1. Sketch of a thrust chamber inner contour with relevant geometric parameters.

geometry, each specific design may require dedicated testings. This is the main reason for the continuous characterization of the hot-gas side heat transfer over the years. Many of these studies, with associated experimental data, are the basis of this work and therefore will be described and analyzed in the final sections.

In addition to the experimental activities, the Computational Fluid Dynamics (CFD) approach can be used to study the problem of the hot-gas side heat transfer. Consequently, such an approach is potentially useful in reducing the development and verification costs of a rocket engine thrust chamber. With the improvement of computing capability since the 1990s, detailed investigations of the hot-gas flow has become affordable. However, extensive parametric analyses are still prohibitive because of the very demanding computational resources required to take into account the multi-dimensional phenomena occurring near the injector (i.e., propellant injection, atomization, evaporation, mixing, and combustion) and the evolution of the chemically reacting, and potentially radiating, combustion products in the convergent–divergent nozzle and near the cooled wall, where large gas temperature gradients are present. Recent efforts in simulating the hot-gas flow, with particular focus on the wall heat transfer, can be found in [6–12]. In [6], a multidimensional numerical solver able to simulate both liquid and gaseous propellant injection, combustion, and expansion through the nozzle is presented. Many assumptions and simplifications are made to make the problem solvable with current computing resources. In [7], a subscale thrust chamber fed with oxygen–methane through an injector having 18 shear-coaxial elements is studied in detail. Results show that non-negligible temperature and heat flux variations are present in the circumferential direction. In [8,9], the effect of chemical recombinations and hot-gas radiation on the wall heat transfer is studied considering a subscale thrust chamber. Results show that oxygen–methane combustion products are subjected to near-wall recombination phenomena, providing an increase of wall heat flux of 20% with respect to a chemically-frozen flow and a decrease of 5% with respect to a flow in chemical equilibrium. In the case of oxygen–hydrogen combustion products, wall recombinations occur essentially in chemical equilibrium, implying a wall heat flux increase of 10% with respect to a chemically-frozen flow. The radiative contribution to the heat flux in the cylinder portion of a thrust chamber is evaluated to be up to 15% for oxygen–methane and 11% for oxygen–hydrogen while it is almost negligible in the throat region. In [10], an oxygen–hydrogen fed full-scale thrust chamber is simulated, showing that a

detailed multidimensional simulation of the injection elements and film cooling holes implies a noticeable increase of the throat region heat flux with respect to a simplified and computationally affordable two-dimensional axisymmetric simulation relying on uniform hot-gas injection through the thrust chamber inlet area and a film cooling slot. The wall heat transfer in a small thrust chamber with variable thrust and fed with gaseous oxygen and liquid kerosene through a pintle injector is numerically studied in [11]. Finally, in [12] an oxygen–methane fed subscale thrust chamber is considered to numerically study the effect of the coaxial injection element parameters on the wall heat transfer. Results show that a larger liquid oxygen post thickness and the swirl-coaxial instead of shear-coaxial injection can significantly reduce the heat flux. On the other hand, the effect of the injection elements number is relatively small. It is noteworthy that, despite the substantial progress in numerical simulations, as demonstrated in these studies, realistic experimental data are still required for the verification and the development of numerical design tools.

This manuscript presents a thorough survey of the available experimental data concerning the hot-gas side heat transfer to the throat region of liquid rocket engine thrust chambers. Such literature data are elaborated and used to find suitable heat transfer correlations. Compared to other correlations presented in the past and obtained considering experiments made with specific propellants and configurations of the thrust chamber and the injector, the correlations presented here have the added value of taking into account a high variability of operating conditions. In particular, this permits to find an upper limit of the heat transfer that, thanks to the relatively high number of considered data, is statistically meaningful and thus is useful for a safe design. To refine the proposed correlations, specific propellant combinations for which many data are available, like oxygen–hydrogen and oxygen–hydrocarbons, are considered. This manuscript is organized as follows: Section 2 describes the experimental apparatuses typically used for the heat transfer measurements; Section 3 describes the adopted heat transfer correlations and the main phenomena that they take into account; Section 4 describes how the collected data of heat flux and wall temperature are processed to determine the heat transfer coefficients and the non-dimensional numbers used in the adopted heat transfer correlations; finally, Section 5, representing the main core of this study, contains the discussion on the collected and elaborated data and the proposed heat transfer correlations.

2. Experimental measurement apparatuses

The most adopted apparatus to measure the local wall heat flux distribution is the *calorimeter thrust chamber*. This is a specially designed thrust chamber that consists of several axially segmented and independently cooled circuits. Each circuit usually consists of a few channels which are machined circumferentially on a copper (or copper-base alloy) liner, closed-out with a metallic reinforcement structure, and connected with a common inlet and outlet manifold for the cooling fluid, which is always water. This enables the evaluation of the axial distribution of the heat transferred through the thrust chamber walls by metering the water mass-flow rate and measuring its temperature rise in each circuit. The shorter the axial length of each cooling circuit the finer the axial resolution of the heat flux. A fine resolution is required especially in the throat region, due to the sharp axial gradient of heat flux present there. Calorimeter thrust chambers have been realized with up to 58 independent circuits [13]. The amount of cooling water mass flow rate per segment is chosen in such a way that sufficient high-temperature rise of the cooling fluid (of the order of few tens of kelvin) is achieved during the firing. This is required to keep thermal measurement errors small [14]. For safety reasons, the pressure within the coolant circuits is always chosen above the combustion chamber pressure. This assures that in case of a crack, water is injected into the thrust chamber rather than hot-gas into the cooling loop which would quickly destroy the hardware. Water pressure is typically sufficiently high (of the order of hundreds of bar) also to ensure one-phase flow conditions in the cooling circuits. However, a basically different cooling approach using low coolant pressures (below 100 bar) and allowing flow boiling in the cooling circuits is used sometimes (e.g., [15]). This approach allows a good determination of the wall temperature because of its direct relationship with the boiling critical heat flux but results in higher wall temperature and thus lower operative life [16]. In general, among the various experimental apparatuses, the calorimeter thrust chamber provides the most accurate measurement of the heat flux even if the measurement is insensitive to any circumferential variation because is it an average over the complete surface of each cooling circuit. Note that, apart from the case with boiling water in channels, the calorimeter thrust chambers in their essential definition are not provided by any wall temperature measurements. To provide this information, the test articles can be equipped with thermocouples immersed in the wall material. This is not easy because of the small wall thickness with respect to the typical thermocouple diameter. Moreover, the large temperature gradients within the wall, up to 500 K/mm, lead to large measurement error and represent a challenge for the correct positioning of the thermocouples. Because of the presence of multiple cooling channels, there is also a limitation on the number of temperature measurement points that can be placed along the thrust chamber length. For these reasons, the wall temperature is often numerically estimated using the heat flux data and suitable thermal models or roughly supposed considering similar test apparatuses.

A second type of experimental apparatus, although less used than the previous one, is the *heat-sink thrust chamber*. In this case, the heat flux data at various axial stations are obtained from the numerical reconstruction of the wall temperature history measured by multiple thermocouples positioned within the wall of an uncooled thrust chamber. Such thrust chambers are generally made of copper (or copper-base alloy) and with sufficiently large thickness to increase the thrust chamber thermal capacity and thus the firing time, which is limited because of the continuously increasing wall temperature. A minimum firing time is needed to reach a sort of steady-state of the heat transfer coefficient (although the wall temperature increases and the heat flux decreases with time) and, because of the thermal inertia of the temperature sensors [17], to guarantee sufficient measurement accuracy. Consequently, combustion chamber pressure is typically limited to about 40 bar to limit the heating rates, that is, to both extend the firing time and avoid excessive wall temperature spatial gradients that are detrimental to the measurement accuracy. Unlike the calorimeter thrust chambers, the heat-sink thrust chamber allows local measurements both in the axial and circumferential directions. This feature permits studying phenomena like the multidimensional distribution of heat flux near the injector, that is, where the trace of the injector elements is particularly evident.

As for the accuracy of the data obtained with the experimental apparatuses described above, in general the heat flux measurements are affected by not less than 10% of uncertainty. The uncertainty of the heat transfer coefficient may be even greater than 10% because it is impacted by the uncertainty of both the heat flux and the wall temperature, which is typically not small because the wall temperature is often not measured, but only estimated. Also, it has to be reminded that in case of noticeable circumferential variation of the heat transfer, accuracy of the measurements made with the calorimeter thrust chambers is poor. Some data taken using heat-sink thrust chambers have shown that, as a result of the non-uniform hot-gas mixing dependent on the injector pattern, the circumferential variation of the heat transfer coefficient can be as high as 40% close to the injector and 30% at the throat [18,19]. Furthermore, after long periods of operation at high temperatures the hot-gas side surface of most thrust chambers becomes rougher due to erosion and oxidation. Consequently, increments of up to 25% in the heat extracted from the wall of thrust chambers operating at high pressure were measured [20].

3. Hot-gas side heat transfer correlation

During the design process of a new rocket engine thrust chamber, the engineering approach to predict the hot-gas side heat transfer often consists of using correlations for the Nusselt or the Stanton numbers, primarily as a function of the Reynolds and the Prandtl numbers. Such correlations are based on the evidence that convection is the principal process by which the heat is transferred to the walls of a thrust chamber from the hot-gas. In the case of turbulent flow, which is the most likely hot-gas flow regime in high-performance liquid rocket engine thrust chambers, the heat transfer correlation has commonly the form:

$$Nu = C Re^{0.8} Pr^{0.4} \tag{1}$$

When using the Stanton number, the above correlation takes the form:

$$St = C Re^{-0.2} Pr^{-0.6} \tag{2}$$

since the relation between St and Nu is: $St = Nu/(RePr)$. For a fully-developed turbulent flow of a constant-properties fluid in a constant diameter pipe (i.e., having the boundary layer thickness equal to the pipe radius and no appreciable axial pressure gradients), the reference dimension is taken as the pipe diameter and the coefficient C is considered to be a constant equal to 0.023. Since the conditions of fully-developed flow and constant area do not apply for a convergent–divergent rocket thrust chamber, theoretically, a correlation based on the boundary layer thickness should be considered. This approach is difficult to implement because of the impossibility to establish an effective starting point of the turbulent boundary layer. In fact, different injector configurations induce recirculation of different magnitude and thus boundary layers downstream of them with different characteristics. Anyway, in most heat transfer correlations the local nozzle diameter D is considered as the reference dimension because the boundary layer thickness varies in fairly systematic relation to the local diameter throughout a thrust chamber [21]. The suitability of the correlations (1) and (2) in describing the hot-gas side heat transfer is guaranteed by the experimental fact that the peak heat flux is monotonically increasing with the combustion chamber pressure (that is, with the hot-gas mass flux) to the power of 0.8. This trend holds as well for the remainder of the thrust chamber except for the near injector region where combustion and flow recirculation are the dominant phenomena for the heat transfer [22]. To be noted that, even if the hot-gas radiation is a phenomenon that is not modeled in the expressions (1) and (2), when the heat flux to the wall is determined empirically, the measurements contain both the convective and radiant components. This modeling shortcoming is often acceptable because the radiative heat flux is typically no more than 15% of the convective one in the subsonic portion of the thrust chamber and diminishes further in the transonic and supersonic portions of the thrust chamber as the hot-gas temperature drops throughout the expansion process. At the throat location, where the convective heating is maximum, the radiative component is often negligible. Only in some cases with hydrocarbon fuels, poor combustion efficiency can substantially increase the hot-gas luminosity due to the presence of soot and therefore the radiative heat load [23].

Despite the simple form of the heat transfer correlations (1) and (2), the required non-dimensional numbers can be defined in different ways. A first difference concerns the heat transfer coefficient, which can be related to the temperature or the enthalpy, that is, respectively:

$$h_{g,T} = \frac{q_w}{T_{aw} - T_w} \tag{3}$$

or

$$h_{g,i} = \frac{q_w}{i_{aw} - i_w} \tag{4}$$

where T_w and i_w are the hot-gas temperature and enthalpy at the wall, respectively, and q_w is the hot-gas side wall heat flux. The adiabatic wall variables T_{aw} and i_{aw}, representing the hot-gas temperature and enthalpy at the wall in case of adiabatic flow, are close to the values in the combustion chamber T_0 and i_0, respectively. The difference $T_{aw}-T_w$, as well as $i_{aw} - i_w$, is called the driving potential. To be noted that, for a flow of a constant-properties fluid the convective heat transfer coefficient does not depend on the wall temperature and thus the heat flux varies linearly with the driving potential. As this ideal condition represents the case of interest as a first approximation, the heat transfer coefficient in a rocket engine thrust chamber is typically only mildly dependent on the wall temperature. The heat transfer coefficient $h_{g,T}$ is generally used in the definition of the Nusselt number, that is, $Nu = h_{g,T} D/k$ where k is the hot-gas thermal conductivity, whereas the heat transfer coefficient $h_{g,i}$ is generally used in the definition of the Stanton number, that is, $St = h_{g,i}/(\rho u)$, where ρ is the hot-gas density and u is the hot-gas velocity. The other two non-dimensional numbers are defined as $Re = \rho u D/\mu$ and $Pr = \mu c_p/k$, where μ is the hot-gas viscosity and c_p is the hot-gas specific heat at constant pressure. Because of the large hot-gas temperature variations across the boundary layer and the chemically reacting flow behavior, the definition of a reference state to evaluate the hot-gas variables ρ, c_p, μ, and k is not straightforward. To this aim, a reference enthalpy based on Eckert's method is often adopted [24]. Eckert's reference enthalpy of a given thrust chamber section is an average of the free-stream, the wall, and the adiabatic wall enthalpies (i, i_w, and i_{aw}, respectively): $i_{ref} = 0.28i + 0.5i_w + 0.22i_{aw}$ where i_{aw} in case of turbulent flow is often evaluated as $i_{aw} = i + Pr^{1/3}(i_0 - i)$. The Eckert's reference state changes according to the hypothesis on the chemical reactivity of the hot-gas near the wall. In fact, since the hot-gas in a thrust chamber is typically partially dissociated, chemical recombination reactions in the boundary layer, which are induced by the relatively cold wall temperature, may contribute appreciably to the heat flux to the wall. For this reason, an assessment of the chemical reactions occurring within the boundary layer must be done. Since the description of the flow evolution used in conjunction with heat transfer correlations is generally one-dimensional and steady-state, chemical non-equilibrium is generally not taken into account and the flow is supposed to be chemically frozen or in chemical equilibrium. In the latter case, the use of the driving potential based on the enthalpy (Eq. (4)) is particularly suited as the energy released by chemical recombinations is automatically taken into account in the definition of enthalpy.

Besides the effects related to Reynolds and Prandtl numbers (see the correlations (1) and (2)), the hot-gas side heat transfer in the throat region can be influenced by the geometric parameters that are schematically represented in Fig. 1. In particular, the flow turning in the throat region slightly shifts the location of the sonic condition (that is, the condition of maximum mass flux) upstream the throat, where the boundary layer thickness is smaller. This implies an increase of the peak heat transfer with respect to the ideal condition having the sonic condition at the throat section. More specifically, the smaller the ratio of the radius of curvature just upstream the throat to the throat diameter, $\frac{R_c}{D_t}$, and the steeper the convergent angle, θ_c, the larger the flow turning and thus the larger the peak heat flux. In addition, the flow distortion induced by the flow turning in the transonic region also impacts negatively the throat effective area [3]. However, to be noted that increasing $\frac{R_c}{D_t}$ and reducing θ_c reduce the peak heat flux but result in a protracted region of high heat input because the wall surface length of the transonic region is larger [25]. The contraction ratio, $\varepsilon_c = \frac{A_{cyl}}{A_t}$, defining the hot-gas velocity in the combustion chamber and thus the stability of the boundary layer growth as well as the level of mixing in the developing combustion flow field, can also play a role in the location and amount of the peak heat transfer. To be noted that, even if the peak heat transfer occurs upstream the throat, the correlations predict the peak at the throat geometric section because, in agreement to the usually adopted one-dimensional flow description, the maximum mass flux occurs at the minimum area. Finally, thrust chambers of sufficient length (measured as the injector-to-throat distance $L_{cyl}+L_{conv}$ or, more properly, as the characteristic length $L^* = \frac{V_c}{A_t}$) allow a more uniform circumferential throat heat transfer because the effects induced by the non-uniform combustion and the injector streaking are

sufficiently upstream [25]. However, when fitting the heat transfer with experimental data, the geometric effects that can be added to the correlations (1) and (2) reduce to those related to $\frac{R_c}{D_t}$, θ_c, and ε_c because the experimental measurements are often an average value over the circumference.

4. Data reduction

In this study, the experimental data relevant to the peak heat transfer in the throat region are used to properly select the coefficient C of the correlations (1) and (2) by minimization of the error between the experimentally evaluated Nusselt or Stanton number and the computed ones. When geometric data of the tested thrust chambers are available, the geometric term $G = \left(\frac{R_c}{D_t}\right)^{\alpha} \theta_c^{\beta} \varepsilon_c^{\gamma}$ is added to the correlations (1) and (2), where the exponents α, β, and γ are fit to the experimental data by least-square minimization of the Nusselt or Stanton number error. To be noted that, although the correlations found in this way apply strictly to the throat region, they can be used as a first attempt for the other thrust chamber sections as well [5].

Three different approaches of increasing complexity are considered in the present study to evaluate the non-dimensional numbers Nu or St, Re, and Pr: (i) hot-gas properties evaluated at the free-stream state, that is, outside the boundary layer; (ii) hot-gas properties evaluated at the Eckert's reference state considering frozen chemical composition in the boundary layer; and (iii) hot-gas properties evaluated at the Eckert's reference state considering chemical equilibrium in the boundary layer. All three of these approaches are based on the same input data coming from the experimental measurements: the combustion chamber pressure p_0, the oxidizer-to-fuel mass mixture ratio o/f, the characteristic velocity c^*, and the hot-gas side wall heat flux q_w and wall temperature T_w. When multiple measurements of throat section q_w and T_w are provided for the same fire test, the values providing the maximum and minimum heat transfer coefficient are used to define the range, rather than a unique value, of the dimensionless numbers associated with that test. Multiple measurements are common with heat-sink thrust chambers (Section 2), as different circumferential positions or different times are often considered in this case. When the wall temperature is not measured, which is typical of calorimeter thrust chambers (Section 2), the range of the dimensionless numbers associated with each test is evaluated considering the minimum and the maximum expected wall temperature. If this range is not provided by the experimentalists, a rather large assumption is made, considering that the wall temperature at the throat is between 600 and 900 K. For what concerns the evaluation of the characteristic velocity c^*, when the experimental data of the propellant mass flow rate $\dot{m}$ is available, it is computed as $c^* = p_0 A_t / \dot{m}$. Otherwise, if only the combustion efficiency η_{c^*} is known, the characteristic velocity is computed as $c^* = \eta_{c^*} c^*_{id}$ where c^*_{id} is the ideal characteristic velocity. It is computed considering a one-dimensional isentropic expansion through the thrust chamber of the hot-gas in chemical equilibrium [26,27]. The input data for the evaluation of c^*_{id} are p_0, o/f, and the inlet temperature of the propellant. Details of the three calculation procedures are provided below for the case of interest, which is the throat region heat transfer. Obviously, the following procedures can be immediately extended to the other sections of the thrust chamber. The turbulent boundary layer hypothesis is considered valid.

4.1. Formulation based on hot-gas properties evaluated at the free-stream state

A one-dimensional isentropic expansion from the inlet section, considered with an infinite area, up to the throat of the hot-gas in chemical equilibrium is computed considering the known values of p_0 and o/f, and a proper value of the propellant inlet enthalpy i_0 such to match the experimental value of c^*. The resulting hot-gas properties u, ρ, c_p, μ, and k at the throat section are used to evaluate the non-dimensional numbers Nu_∞, Re_∞, and Pr_∞ to be used in (1), where the subscript "∞" indicates that the hot-gas variables are the free-stream ones. The adiabatic wall temperature T_{aw} to be used in the definition of $h_{g,T}$ (Eq. (3)) and thus in Nu_∞ is estimated as $T_{aw} = T + Pr_\infty^{1/3}(T_0 - T)$, where T is the hot-gas free-stream temperature at the throat section and T_0 is the combustion chamber temperature. Note that this formulation has the great advantage, with respect to the following ones, of requiring minimum thermodynamic computations.

4.2. Formulation based on hot-gas properties evaluated at the Eckert's reference state considering frozen chemical composition in the boundary layer

In this case, the hot-gas properties at the throat section are evaluated at a reference state defined by the pressure p and the Eckert's reference enthalpy $i_{ref} = 0.5(i + i_w) + 0.22 Pr_\infty^{1/3}(i_0 - i)$. Note that the properties p, i, and Pr_∞ are the throat free-stream properties, i_0 is the propellant inlet enthalpy, all evaluated as indicated in Section 4.1 (that is, considering the free-stream in chemical equilibrium), and i_w is the enthalpy of the hot-gas at the throat free-stream pressure p and wall temperature T_w. Calculations are made considering that the hot-gas composition in the boundary layer is equal to the free-stream one (i.e., frozen chemical composition). The resulting non-dimensional numbers to be used in (2) are St_f, Re_f, and Pr_f, where the subscript "f" indicates that the hot-gas is considered at frozen chemical composition in the boundary layer. Note that the hot-gas velocity u to be used in the definition of St_f and Re_f is the free-stream one, as evaluated in Section 4.1, and that the adiabatic wall enthalpy i_{aw} to be used in the definition of $h_{g,i}$ (Eq. (4)) and thus in St_f is estimated as $i_{aw} = i + Pr_f^{1/3}(i_0 - i)$.

4.3. Formulation based on hot-gas properties evaluated at the Eckert's reference state considering chemical equilibrium in the boundary layer

This approach is similar to the previous one but the hot-gas is considered in chemical equilibrium also in the boundary layer. This implies a different evaluation of i_w and thus i_{ref}. The chemical equilibrium condition is then found at the throat free-stream pressure p and the reference enthalpy i_{ref} to define the reference variables. Such variables are used to evaluate the non-dimensional numbers St_e, Re_e, and Pr_e to be used in (2), where the subscript "e" indicates that the variables take into account that the hot-gas in the boundary layer is in chemical equilibrium.

Among the throat heat transfer data found in the literature, only those satisfying the following conditions are considered for this study: (i) steady-state heat transfer; (ii) turbulent flow; (iii) no evident soot deposition; (iv) uniform injection. The identification of these conditions is not always straightforward. Therefore the selected data may partially not satisfy the four conditions listed above. In what follows, a methodological discussion on how the data have been selected is given. For what regards condition (i), steady-state heat transfer is the normal condition in the case of calorimeter thrust chambers while in the case of heat-sink thrust chambers, even if the wall temperature increases and the heat flux decreases with time, heat transfer coefficient reaches a sort of steady-state (Section 2). When possible, the latter condition has been verified. For what regards conditions (ii), data with Re_∞ below about 200,000 are discarded. In fact, in [28] it is suggested that below a throat Reynolds number of 200,000 the nozzle flow is laminar while in the range between 200,000 and 400,000 the flow may be laminar, transitional, or turbulent, depending on nozzle geometry and combustion effects. For what regards conditions (iii), to avoid the inclusion of heat transfer data affected by solid carbon (i.e., soot) deposition, only experiments that did not show visual evidence of carbon buildup during the post-test inspection and with stable heat flux with time are taken. In fact, when soot is present, the heat flux decreases with

Table 1
Summary of the selected references containing experimental measurements of the throat heat transfer, divided by propellant combinations.

Propellants	No. of data	No. of independent setups	References
O_2–H_2	125	16	[13,15,17–19,23,30–39]
O_2–kerosene	61	9	[15,40–47]
O_2–CH_4	36	4	[15,44,48,49]
O_2–C_2H_5OH	15	1	[50]
O_2–C_3H_8	9	1	[50]
O_2–NH_3	14	1	[51]
HNO_3–NH_3	35	1	[52]
N_2O_4–N_2H_4	41	3	[53–56]
F_2 + O_2–CH_4	13	1	[57]
F_2 + O_2–CH_4 + C_2H_6	73	1	[58]
F_2–H_2 + Li	9	1	[59]
Air	57	3	[21,60–62]
	total = 488	total = 42	

time as a result of the increasing thickness of the carbon deposition at the wall [29]. Obviously, even if this approach permits to discard the cases with evident soot formation, when using heavy hydrocarbons like kerosene, a certain presence of soot is always possible. This possibility will be discussed in detail in the next Section 5.2. Finally, to respect condition (iv), test cases with film cooling or intended non-uniform injection (e.g., propellant mixture ratio bias) that affect the throat heat transfer are discarded. Such injection configurations are sometimes easily identifiable as the heat transfer with and without uniform injection has been compared in some test campaigns (e.g., [23]).

With the above-described logic, a total number of 488 tests are selected. Table 1 summarizes the whole data set, divided by propellant combinations. For each propellant combination, the number of collected data is reported, as well as the number of the employed independent setups (that is, the number of different experimental apparatuses). The references providing the original data are also indicated. Looking at Table 1, it is evident that most of the experiments are relevant to the widely used oxygen–hydrogen and oxygen–kerosene propellant pairs. Few test campaigns involving oxygen–methane have been carried out in the late 1980s and involving nitrogen tetroxide–hydrazine in the 1960s. The other propellants have been tested in single experimental campaigns. For those data, the lack of a comparison with independent experimental apparatuses represents a criticality for their reliability and reproducibility. A peculiar case, already discussed in Section 1, is that of experiments using air as it is not a rocket propellant. For this reason, such data are not treated in detail in the following analysis.

5. Data analysis

The whole set of experimental data is presented in Figs. 2, 3, and 4 in suitable plots having the Reynolds number and the Nusselt (or Stanton)–Prandtl numbers group in the axis, in agreement with the correlations (1) and (2). Data are grouped by type of propellants. Note that the data characterized by a range of non-dimensional numbers rather than a unique value, as described in Section 4, are plotted as a couple of linked points representing the minimum and maximum values. Note also that logarithmic plots are used to represent the heat transfer correlations as parallel straight lines having a slop equal to the Reynolds number exponent (i.e., 0.8 in case of Re_∞ and −0.2 in case of Re_f or Re_e) and different intercepts with varying coefficient C. In each plot, two lines associated with two different coefficients C are drawn: the first one, indicated as "fit", represents the correlation that minimizes the error with respect to the experimental data; the second one, indicated as "$+2\sigma$", represents the correlation that includes the 95.45% of the data. The latter value may be useful in the design phase of a thrust chamber for which no specific heat transfer measurements are known. In fact, using the correlation with $C_{+2\sigma}$ guarantees, with sufficient margin, that the real hot-gas side heat transfer coefficient is not higher. To be noted that in case of large data scattering (i.e., large difference between C_{fit} and $C_{+2\sigma}$) a design made using $C_{+2\sigma}$ may be inefficient because too conservative. The general comment on Figs. 2, 3, and 4 is that the data are quite scattered as $C_{+2\sigma}$ is larger than C_{fit} by 68%, 55%, and 55%, respectively. Consequently, it is not easy to identify the best choice for the reference variables to be used in the heat transfer correlations. The large data scattering is probably the consequence of having considered extremely different propellant combinations and injector configurations. Moreover, in a test campaign using the same propellant the injector is often tested with small geometric modifications from test to test to study their effect on the combustion efficiency, combustion stability, and heat transfer. Finally, also the generally non-negligible measurement error must be considered as a source of data scattering. To better analyze these plots and the reason for the large data scattering, some specific behaviors must be highlighted. The numerous data coming from the single source [58] and pertinent to FLOX (i.e., a blend of F_2 and O_2) and LPG (i.e., a blend of 55% CH_4 and 45% C_2H_6) propellant combination are grouped in a narrow range of Reynolds number (i.e., testing are made at similar combustion chamber pressure and mixture ratio conditions) but show very poor reliability and reproducibility, that is, heat transfer data are very scattered. The data relevant to nitric acid (HNO_3) and ammonia (NH_3) propellant combination [52] are probably affected by a bias error originating from the fact that the adopted calorimeter thrust chamber has a rather wide coolant circuit in the throat region, that is, the measured average value is noticeably lower than the real peak value. The data relevant to the tripropellant combination of fluorine (F_2), hydrogen (H_2), and lithium (Li) [59] must be treated with care as the adopted experimental apparatus is rather unconventional. It consists of a gas generator operating with F_2 and H_2 while the third propellant (Li) is injected downward. Moreover, the combustion product lithium fluoride (LiF) may condense on the wall in the solid phase and the unburnt lithium in the liquid phase, making the heat transfer mechanism not easily comparable with that of the other data. Nitrogen tetroxide (N_2O_4) and hydrazine (N_2H_4) data are obtained employing unconventional injectors with respect to those used for the other propellants. In particular, when using a single-element pintle injector [56] the heat transfer is noticeably lower than when using a splash ring plate that promotes strong recirculation of the hot-gas and low combustion efficiency [53–55]. Finally, Boldam and al. [61,62] collected heat transfer data of heated air in converging–diverging nozzle having different values of surface roughness and different origin of the thermal boundary layer (using cooled or uncooled portions of the cylinder upstream the nozzle). Consequently, for the same flow conditions at the throat (i.e, the same Reynolds number), the heat transfer coefficient results to be very variable.

To find more reliable data regressions, in the following subsections the data are analyzed more closely considering homogeneous propellant combinations. Since the dispersion of the data does not change much depending on how the reference variables are calculated, only the plots relevant to the free-stream variables will be presented in the following subsections. However, in the final Section 5.3, the three different approaches to evaluate the hot-gas properties and relevant coefficients C are discussed in detail.

5.1. Oxygen–hydrogen propellant

The first group of homogeneous data analyzed in detail is relevant to the oxygen (O_2) and hydrogen (H_2) propellant combination. A total number of 125 data from 16 independent experimental setups are collected. For each reference, Table 2 reports the number of the selected data, the adopted injector type (in some cases more than one), the thrust chamber type, the combustion chamber pressure range of the experiments, how the heat flux and the wall temperature are estimated, and additional notes (such as the accuracy and the reliability of the

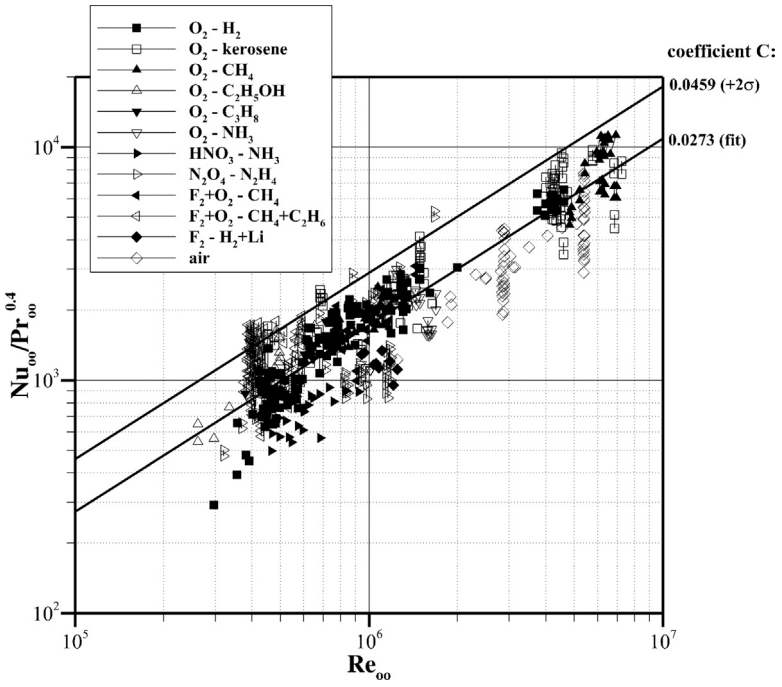

Fig. 2. Throat heat transfer behavior of the whole data set, grouped by type of propellants, in terms of non-dimensional numbers evaluated using free-stream hot-gas properties.

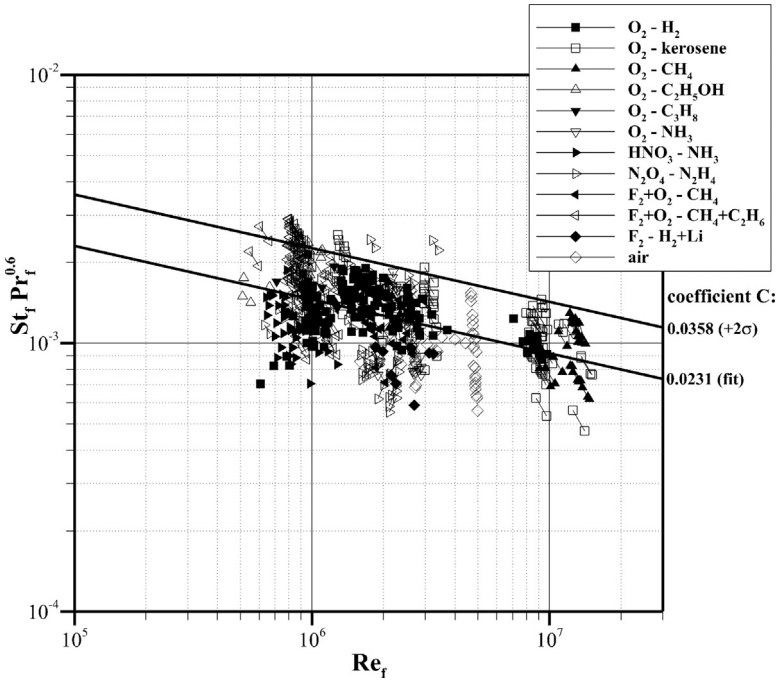

Fig. 3. Throat heat transfer behavior of the whole data set, grouped by type of propellants, in terms of non-dimensional numbers evaluated using the Eckert's reference state under the hypothesis of hot-gas with frozen chemical composition.

data and the assumed range of the wall temperature). It is possible to note that the range of combustion chamber pressure is rather wide, being from 15 to 127 bar, and that almost all the adopted injectors are based on axial or coaxial elements (with possible swirling). The adoption of similar injectors adds consistency to the analyzed data. Concerning the type of thrust chambers, both calorimeter and heat sink thrust chambers have been extensively employed. Note that, when combustion chamber pressure exceeds about 40 bar only calorimeter thrust chambers can be used because of the excessive heat load to the wall (Section 2). Finally, in Table 2 some cases with unconventional thrust chamber design are associated with potentially low data reliability.

The O_2-H_2 heat transfer data using free-stream hot-gas properties are presented in Fig. 5 using the same plot type of Fig. 2. In this case, the data are grouped by the literature source. With respect to the plot containing the whole data set, (Fig. 2), the value of the coefficient C_{fit} is very similar while the difference between the coefficients C_{fit} and $C_{+2\sigma}$ halves, passing from 68% to 34%, as a result of a much lower data dispersion. It is also worth noting that the data of [35] with relatively low Reynolds number may be affected by laminar or transitional flow

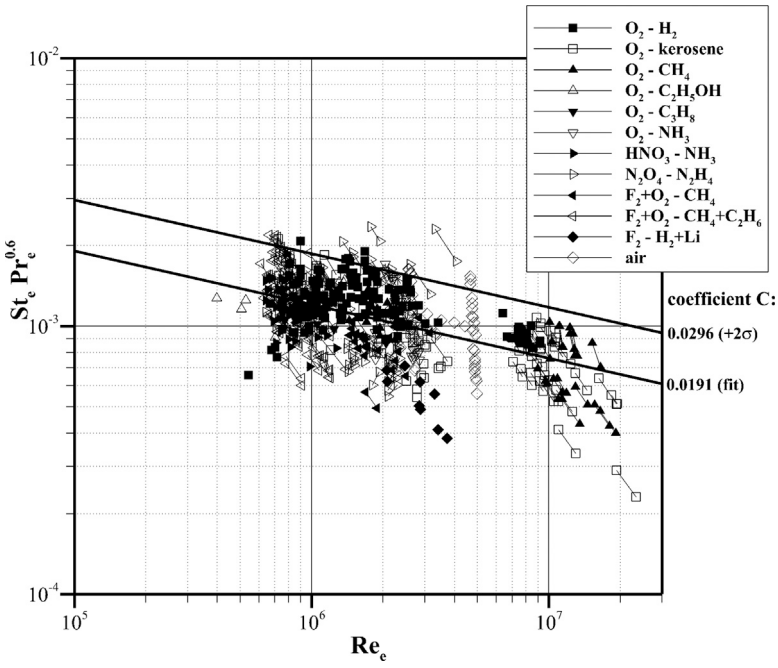

Fig. 4. Throat heat transfer behavior of the whole data set, grouped by type of propellants, in terms of non-dimensional numbers evaluated using the Eckert's reference state under the hypothesis of hot-gas in chemical equilibrium.

Table 2
Selected references containing throat heat transfer data of oxygen–hydrogen fed thrust chambers.

O_2–H_2							
Reference, Country, Year	No. of data	Injection type[a]	Chamber pressure [bar]	Chamber type[b]	Heat flux evaluation[c]	Wall temperature evaluation[c]	Notes
[18], USA, 1971	5	CP, CO	21	HS	computed	measured	multiple circumferential data (up to 30%h_c variation); declared T_w accuracy 5% and h_c accuracy 8%
[30], USA, 1972	2	CP	21–43	HS	computed	measured	
[19], USA, 1973	22	PT, SC, CO	19–33	HS	computed	measured	multiple circumferential data (up to 30%h_c variation)
[31], USA, 1973	1	CP	51	CA	measured	expected	declared h_c accuracy 10%
[32], USA, 1973	6	TR	15–19	HS	computed	measured	declared q_w accuracy 10%
[33], USA, 1973	6	CP	26–49	CA	measured	assumed	assumed T_w range: 600–900 K
[34], USA, 1986	24	SC	26–47	CA	measured	evaluated	low data reliability (dual throat chamber)
[35], USA, 1988	7	PT	27–41	HS	computed	measured	low data reliability (centerbody chamber)
[36], USA, 1991	10	SF	102–116	CA	measured	expected	
[37], USA, 1993	7	AP	40–42	CA	measured	measured	low data reliability (plug chamber)
[23], USA, 1993	9	SP, SH, SB	122–127	CA	measured	exp. / ass.	when T_w is not declared, it is assumed as 600–900 K
[13], USA, 2004	1	CP	109	CA	measured	computed	
[38], Japan, 1982	9	CF	28–35	CA	measured	measured	T_w indirect measurement by water nucleate boiling
[15], Japan, 1990	10	CC	71–95	CA	measured	measured	T_w indirect measurement by water nucleate boiling
[17], Germany, 1993	1	CP	30	–	expected	expected	details of experimental apparatus not declared
[39], Germany, 2006	5	CO	35–70	CA	measured	assumed	assumed T_w range: 600–900 K

[a]CP = coaxial elements with residual fuel through porous faceplate; CO = coaxial elements; PT = premix triplet elements; SC = swirler coaxial elements; TR = unlike impinging triplet elements; SF = swirler coaxial elements with residual fuel through peripheral holes; AP = oxidizer axial elements and fuel through porous faceplate; SP = swirler coaxial elements with residual fuel through porous faceplate; SH = swirler coaxial elements with residual fuel through porous faceplate and peripheral holes; SB = swirler coaxial elements with mixture ratio bias and residual fuel through porous faceplate; CF = coaxial elements with residual fuel through peripheral holes; CC = coaxial elements with residual fuel through porous faceplate and peripheral holes.

[b]HS = heat-sink thrust chamber; CA = calorimeter thrust chamber.

[c]**measured** = experimentally measured data; **computed** = computed data, taken from the original reference; **expected** = expected data, taken from the original reference; **assumed** = data not provided in the original reference and thus assumed within this study.

conditions as the Nusselt number is noticeably lower than the rest of the data.

The relatively large availability of the O_2-H_2 experiments permits the selection of a statistically representative data set that is supplied with detailed information on the thrust chamber geometry, namely, the radius of curvature upstream the throat, the contraction ratio, and the convergent angle. Such set, composed of 68 data, permits to refine the regression with the additional geometric term $G = \left(\frac{R_c}{D_t}\right)^{\alpha} \theta_c^{\beta} \varepsilon_c^{\gamma}$, as discussed in Section 4. The range of the geometric parameters is: $0.5 < \frac{R_c}{D_t} < 1$; $17° < \theta_c < 45°$ (for most of the data the upper limit is 30°); and $3.3 < \varepsilon_c < 12$ (for most of the data the upper limit is 5.6). The resulting fit coefficients using free-stream properties are: $C_{fit} = 0.0464$, $C_{+2\sigma} = 0.0545$, $\alpha = -0.239$, $\beta = 0.319$, and $\gamma = -0.231$, where the convergent angle θ_c is measured in radians. The improvement with respect to the case of Fig. 5 is evidenced by the reduced difference between C_{fit} and $C_{+2\sigma}$, which is now about 18%. In judging this value, it should be considered that a correlation able to contains within ±20% of uncertainty the experimental data coming from different experimental apparatuses and different experimentalists is probably the best that can be achieved, also considering the often non-negligible error of the

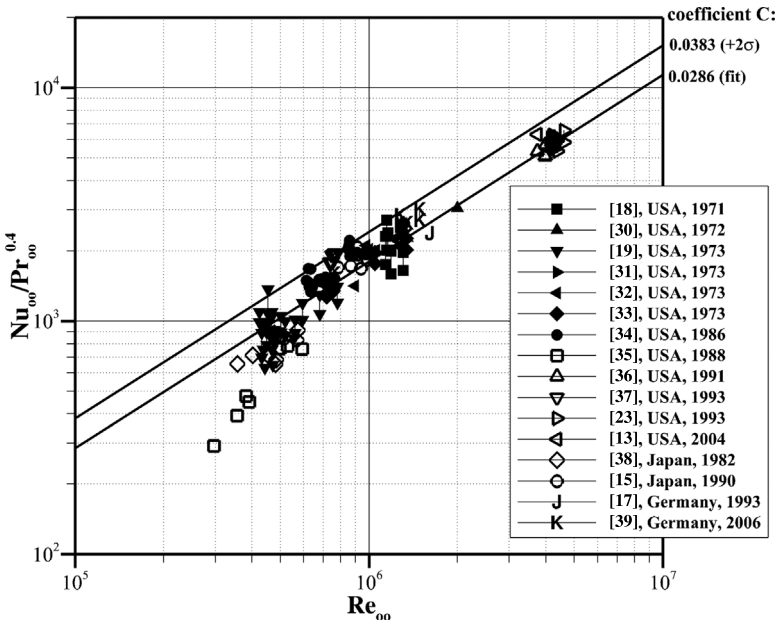

Fig. 5. Throat heat transfer behavior of the data relevant to the O_2-H_2 propellant, grouped by literature source, in terms of non-dimensional numbers evaluated using free-stream hot-gas properties.

Table 3
Selected references containing throat heat transfer data of oxygen–kerosene (mostly RP-1) fed thrust chambers.

O_2–kerosene (mostly RP-1)							
Reference, Country, Year	No. of data	Injection type[a]	Chamber pressure [bar]	Chamber type[b]	Heat flux evaluation[c]	Wall temperature evaluation[c]	Notes
[40], USA, 1980	3	TA	136–137	CA	measured	expected	expected T_w range: 700–811 K
[41], USA, 1985	3	TD	119–153	CA	measured	assumed	assumed T_w range: 600–900 K
[42], USA, 1987	4	TR	71–105	CA	measured	measured	peculiar chamber with small D_t (12.7 mm) and high L^* (~ 15 m)
[43], USA, 1988	7	TR	43–44	CA	measured	assumed	assumed T_w range: 600–900 K
[44], USA, 1990	11	DO	141–159	CA	measured	assumed	assumed T_w range: 600–900 K
[45], USA, 1991	7	DT, AD, TR DO, DB	122–144	CA	measured	assumed	assumed T_w range: 600–900 K
[46], USA, 1991	5	TR	67–105	CA	measured	assumed	assumed T_w range: 900–1100 K (same range of [42] because same apparatus)
[15], Japan, 1990	19	TR	51–104	CA	measured	measured	T_w indirect measurement by water nucleate boiling; fuel is RJ-1J, not RP-1
[47], Korea, 2006	2	SC	53–61	CA	measured	measured	fuel is Jet-A1, not RP-1

[a]TA = unlike impinging pre-atomized triplet elements; TD = unlike impinging pre-atomized doublet elements in the outer rings and unlike impinging pre-atomized triplet elements in the inner rings; TR = unlike impinging triplet elements; DO = like impinging doublet elements arranged in concentric alternating rings; DT = like impinging doublet and unlike impinging triplet elements arranged in concentric alternating rings; AD = oxidizer through axial elements and fuel through like impinging doublet elements; DB = alternating like impinging doublet elements; SC = swirler coaxial elements.

[b]CA = calorimeter thrust chamber.

[c]**measured** = experimentally measured data; **expected** = expected data, taken from the original reference; **assumed** = data not provided in the original reference and assumed within this study.

experimental measurements. For what concerns the effect of the added geometric terms, as partially discussed in Section 3, the heat transfer decreases when the relative radius of curvature upstream the throat increases, the convergent angle decreases, and the contraction ratio increases. With respect to the widely used Bartz's formulation having $\alpha = -0.1$ [5], the current formulation ($\alpha = -0.239$) dictates more than double the effect of the radius of curvature upstream the throat.

5.2. Oxygen–hydrocarbon propellants

The second group of homogeneous data analyzed in detail is relevant to oxygen–hydrocarbon propellants. The hydrocarbons that have been considered as a fuel in conjunction with O_2 to characterize the hot-gas side heat transfer are kerosene, methane (CH_4), ethanol (C_2H_5OH), and propane (C_3H_8). In particular, data relevant to kerosene, mostly in the refined form named RP-1, and CH_4 have been collected with multiple and independent experimental studies (Table 1). RP-1 has an approximate chemical formula of $C_{11.8}H_{23.0}$ and thus, unlike the other fuels considered in this section, is considered a heavy hydrocarbon because of its relatively high molar mass of 164.6 g/mol [63]. In comparison, molar mass of CH_4 is 16.04 g/mol, of C_2H_5OH is 46.07 g/mol, and of C_3H_8 is 44.1 g/mol. The references of the heat transfer data relevant to kerosene are summarized in Table 3 and those relevant to light hydrocarbons in Table 4. These Tables have the same structure of Table 2, which is described in the previous Section 5.1. Unlike the cases with O_2-H_2 propellants (Table 2), the injectors used with kerosene, C_2H_5OH, and C_3H_8 are based on impinging elements, albeit with multiple configurations. On the other hand, coaxial elements (with possible swirling) are used in the case of O_2-CH_4. This selective choice of the injector elements is made because propellant atomization and mixing is more easily assessed with direct impinging when the fuel is injected in the liquid state (like in the case of kerosene, C_2H_5OH, and

Table 4
Selected references containing throat heat transfer data of oxygen–light hydrocarbon fed thrust chambers.

O_2–light hydrocarbons								
Reference, Country, Year	Fuel	No. of data	Injection type[a]	Chamber pressure [bar]	Chamber type[b]	Heat flux evaluation[c]	Wall temperature evaluation[c]	Notes
[48], USA, 1988	CH_4	8	SC	101–159	CA	measured	assumed	assumed T_w range: 600–900 K
[49], USA, 1989	CH_4	1	CO	139	CA	measured	assumed	assumed T_w range: 600–900 K
[44], USA, 1990	CH_4	7	CP	136–143	CA	measured	assumed	assumed T_w range: 600–900 K; assumed η_{c*} range: 97.5–99.5 %
[15], Japan, 1990	CH_4	20	CC	35–96	CA	measured	measured	T_w indirect measurement by water nucleate boiling
[50], USA, 1983	C_2H_5OH	15	TR, TA	10–26	CA	measured	expected	no soot evidence
[50], USA, 1983	C_3H_8	9	TR	14–28	CA	measured	expected	data taken during the first seconds after ignition, when soot is not yet accumulated at wall

[a]SC = swirler coaxial elements; CO = coaxial elements; CP = coaxial elements with residual fuel through porous faceplate; CC = coaxial elements with residual fuel through porous faceplate and peripheral holes; TR = unlike impinging triplet elements; TA = unlike impinging pre-atomized triplet elements.
[b]CA = calorimeter thrust chamber.
[c]**measured** = experimentally measured data; **expected** = expected data, taken from the original reference; **assumed** = data not provided in the original reference and assumed within this study.

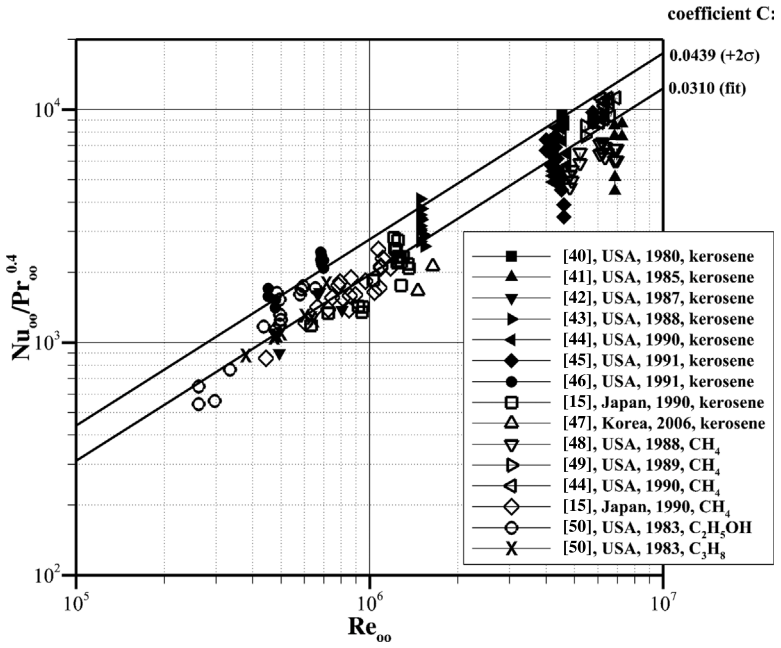

Fig. 6. Throat heat transfer behavior of the data relevant to the O_2-hydrocarbon propellants, grouped by literature source, in terms of non-dimensional numbers evaluated using free-stream hot-gas properties.

C_3H_8). On the other hand, when the fuel is injected in the gaseous state (like in case of CH_4 or H_2), coaxial elements are preferred. Tables 3 and 4 indicate also that all the experimental measurements are made using calorimeter thrust chamber. The use of heat-sink thrust chambers is in fact impracticable due to the relatively high combustion chamber pressure of most of the performed tests. Consequently, since wall temperature measurement is hardly available (see Section 2), this value has been assumed for many test cases. Furthermore, for one test campaign with CH_4 as fuel [44], due to the lack of information on both the propellant mass flow rate and the combustion efficiency, the heat transfer coefficients are evaluated assuming a credible range of combustion efficiency.

The 121 oxygen–hydrocarbon heat transfer data using free-stream hot-gas properties are presented in Fig. 6 using the same plot type of Fig. 2. In this case, the data are grouped by the literature source and employed fuel. It is possible to recognize in the region of high Reynolds number the data of kerosene and methane having a combustion chamber pressure up to about 160 bar, while in the region of low Reynolds number the data of C_2H_5OH having a combustion chamber pressure as low as 10 bar. Although different propellants and a relatively wide range of combustion chamber pressure are considered, the heat transfer behavior is fairly consistent, that is, the Nusselt number correlates with the Reynolds number as foreseen by (1). With respect to the case considering the whole data set (Fig. 2), the coefficient C_{fit} in Fig. 6 is only 14% larger. For what concerns the dispersion of the data, the difference between the coefficients C_{fit} and $C_{+2\sigma}$ is about 42%, which is 12% more than in case of O_2-H_2 (Fig. 5). Unfortunately, due to the absence of the geometric data of many of the calorimeter thrust chambers used with O_2-hydrocarbon propellants, correlations including geometric parameters, as done in the case of O_2-H_2 (Section 5.1), are not considered. A careful analysis of Fig. 6 shows that the most scattered data are those relevant to kerosene. A possible explanation is the wide variability of adopted injectors (Table 3), which can have a significant effect on the wall heat transfer up to the thrust chamber throat, as well as the presence of soot, which can induce wall insulation and increased luminescence of the hot-gas and thus may cause variability of the heat transfer from case to case. Note that a certain presence of soot cannot be excluded a priori although the data selected and summarized in Table 3 are not significantly affected by this phenomenon (Section 4). To improve the heat transfer correlation when dealing with kerosene,

Table 5
Coefficients of the throat heat transfer correlations for different propellant combinations and hot-gas reference variables.

Data set	Free-stream: $Nu_\infty = C Re_\infty^{0.8} Pr_\infty^{0.4}$			Frozen chemistry: $St_f = C Re_f^{-0.2} Pr_f^{-0.6}$			Chemical equilibrium: $St_e = C Re_e^{-0.2} Pr_e^{-0.6}$		
	C_{fit}	$C_{+2\sigma}$	$\frac{C_{+2\sigma}-C_{fit}}{C_{fit}}$	C_{fit}	$C_{+2\sigma}$	$\frac{C_{+2\sigma}-C_{fit}}{C_{fit}}$	C_{fit}	$C_{+2\sigma}$	$\frac{C_{+2\sigma}-C_{fit}}{C_{fit}}$
All	0.0273	0.0459	68.1%	0.0231	0.0358	55.0%	0.0191	0.0296	55.0%
O_2-H_2	0.0286	0.0383	33.9%	0.0237	0.0316	33.3%	0.0217	0.0288	32.7%
O_2-hydrocarbons	0.0310	0.0439	41.6%	0.0253	0.0358	41.5%	0.0181	0.0251	38.7%
O_2-kerosene	0.0311	0.0459	47.6%	0.0251	0.0370	47.4%	0.0174	0.0261	50.0%
O_2-CH_4	0.0296	0.0372	25.7%	0.0244	0.0304	24.6%	0.0187	0.0237	26.7%

the effect of parameters that may be related to the presence of soot, like propellant mixture ratio o/f, combustion chamber pressure p_0, and combustion efficiency η_{c^*}, have been tentatively added in the heat transfer correlations (1) and (2). The most convincing correlation is the one having only the term o/f. The minimum and maximum o/f of the experimental O_2-kerosene data are 1.76 and 3.74, respectively. The best fit correlation indicates that the heat transfer coefficient increases almost linearly with the mixture ratio. This is qualitatively consistent with the fact that the larger the amount of kerosene relative to the oxidizer (i.e., the lower the o/f) the larger the soot deposition at the wall (i.e., the larger the wall thermal insulation). The details of such correlation are given in the next section.

5.3. Resume of the heat transfer correlations

The values of the best-fit coefficient (C_{fit}) and the coefficient including 95.45% of the data ($C_{+2\sigma}$), to be used with the correlations (1) and (2), for various propellant combinations are summarized in Table 5. The relative difference between these values is also summarized in the table to appreciate the dispersion of the experimental data. In addition to the cases discussed in the above sections, the subsets pertaining to O_2-kerosene and O_2-CH_4 are presented. The analysis of Table 5 shows that, when using free-stream or frozen-composition properties, C_{fit} does not change much depending on the propellant considered. When using chemical-equilibrium properties, the variation of C_{fit} is limited to about 20%. In general, for a given propellant combination, C_{fit} is minimum when using chemical-equilibrium properties and is maximum when considering free-stream properties. The intermediate case, that is when using frozen-composition properties, is the one closer to the coefficient 0.023 used in the classic Dittus-Boelter correlation. It is worth noting that, comparing the cases having H_2, kerosene, and CH_4 as fuels, C_{fit} of O_2-kerosene is more than 10% higher than in case of O_2-H_2 when using the free-stream or frozen-composition properties. On the contrary, C_{fit} of O_2-kerosene is about 20% lower than in case of O_2-H_2 when using chemical-equilibrium properties. In any case, C_{fit} of O_2-CH_4 is in between the cases of O_2-kerosene and O_2-H_2. As for the difference between C_{fit} and $C_{+2\sigma}$, Table 5 shows that, apart from the case including all the data, $C_{+2\sigma}$ is almost 50% larger than C_{fit} in case of O_2-kerosene, almost 35% larger in case of O_2-H_2, and less than 30% larger in case of O_2-CH_4. Such percentages do not change appreciably depending on the correlation used. This indicates that no correlation is better than the others in terms of experimental data dispersion. On the other hand, the correlation based on the free-stream properties is superior to the others for simplicity of use, while the one based on frozen-composition properties is to be preferred as it shows a minimum variability of C_{fit} depending on the propellant combination considered.

As already discussed in Section 5.1, the O_2-H_2 correlations can be greatly improved by including the geometric term G. In this case the Nusselt and Stanton correlations have the general form:

$$Nu = C Re^{0.8} Pr^{0.4} G \quad \text{and} \quad St = C Re^{-0.2} Pr^{-0.6} G$$
$$\text{where} \quad G = \left(\frac{R_c}{D_t}\right)^{\alpha} \theta_c^{\beta} \varepsilon_c^{\gamma} \tag{5}$$

The whole set of coefficients C_{fit} and $C_{+2\sigma}$ is presented in Table 6. To be noted that the coefficients α, β, and γ do not change appreciably depending on the choice of the reference variables. This is a clear indication that the term G expresses properly the geometry effect, since it must be independent of how the properties of the hot-gas are calculated. The only remarkable difference is that of the exponent α in the case of chemical-equilibrium properties (i.e., the curvature radius effect is less pronounced). However, if the geometric term G is enforced to be equal to that of the free-stream formulation (that is, $\alpha = -0.239$, $\beta = 0.319$, and $\gamma = -0.231$), the chemical-equilibrium coefficients become $C_{fit} = 0.0350$ and $C_{+2\sigma} = 0.0436$, that is, the relative difference C_{fit} and $C_{+2\sigma}$ is still about the same (24.6%). As for the heat transfer correlations pertinent to kerosene, which present a rather high data dispersion (of the order of 50%), a partial improvement is obtained adding the term $S = \left(\frac{o/f}{2.66}\right)^{\delta}$, as discussed in Section 5.2. In this case the Nusselt and Stanton correlations have the general form:

$$Nu = C Re^{0.8} Pr^{0.4} S \quad \text{and} \quad St = C Re^{-0.2} Pr^{-0.6} S$$
$$\text{where} \quad S = \left(\frac{o/f}{2.66}\right)^{\delta} \tag{6}$$

The whole set of coefficients C_{fit} and $C_{+2\sigma}$ is presented in Table 7. In such a way, the relative difference between the coefficients C_{fit} and $C_{+2\sigma}$ reduces by about 10%. The coefficient 2.66 in the term S is chosen so that the coefficients C_{fit} of the O_2-kerosene correlations with and without the term S are almost the same (compare Tables 5 and 7).

6. Conclusion

In this study, a comprehensive literature survey of the experimental activities devoted to the heat transfer measurements in liquid rocket engine thrust chambers is carried out to find simplified rules to evaluate the heat transfer coefficient in the most thermally solicited part of the thrust chamber, that is, the throat region. The interest is directed to the cases where the throat heat transfer is not affected by laminar flow, evident soot deposition, or intended non-uniform propellant injection. About 500 hot-fire tests characterized by different propellant combinations, injector configurations, thrust chamber geometries, and combustion chamber pressures, are selected and analyzed. Although the correlations found in this study are fit to the data pertinent to the throat region, they can be used as a first attempt for the other thrust chamber sections as well. Three different types of heat transfer correlations, based on the Nusselt or the Stanton number evaluated at different hot-gas reference states, are considered. Correlations are found for the whole set of experimental data as well as for more specific propellant combinations, like oxygen–hydrogen and oxygen–hydrocarbons (mainly, kerosene and methane). The general conclusion is that the correlations based on free-stream properties are superior to the others for simplicity of use, while the ones based on frozen-composition properties can be preferred as they have minimum variation depending on the propellant considered. Finally, the correlations based on chemical-equilibrium properties are not better than the others and have the disadvantage of requiring multiple chemical equilibrium calculations. However, because of the relatively high dispersion of the experimental data, it is not easy to assess the superiority of one correlation over the others. Such dispersion, associated with the intrinsic and often non-controllable heat transfer variability from case to case and the non-negligible measurement uncertainty, is such that the heat transfer can be even more than 60% higher than the value achieved fitting

Table 6
Coefficients of the oxygen–hydrogen throat heat transfer correlations including the geometric term $G = \left(\frac{R_c}{D_t}\right)^{\alpha} \theta_c^{\beta} \varepsilon_c^{\gamma}$ (θ in radians) and using different hot-gas reference variables.

Coefficients	Free-stream: $Nu_{\infty} = C Re_{\infty}^{0.8} Pr_{\infty}^{0.4} G$	Frozen chemistry: $St_f = C Re_f^{-0.2} Pr_f^{-0.6} G$	Chemical equilibrium: $St_e = C Re_e^{-0.2} Pr_e^{-0.6} G$
C_{fit}	0.0464	0.0372	0.0346
$C_{+2\sigma}$	0.0546	0.0432	0.0430
$(C_{+2\sigma} - C_{fit})/C_{fit}$	17.7%	16.1%	24.3%
α	−0.239	−0.244	−0.142
β	0.319	0.314	0.302
γ	−0.231	−0.213	−0.207

Table 7
Coefficients of the oxygen–kerosene throat heat transfer correlations including the oxidizer-to-fuel mass mixture ratio term $S = \left(\frac{o/f}{2.66}\right)^{\delta}$ and using different hot-gas reference variables.

Coefficients	Free-stream: $Nu_{\infty} = C Re_{\infty}^{0.8} Pr_{\infty}^{0.4} S$	Frozen chemistry: $St_f = C Re_f^{-0.2} Pr_f^{-0.6} S$	Chemical equilibrium: $St_e = C Re_e^{-0.2} Pr_e^{-0.6} S$
C_{fit}	0.0311	0.0251	0.0174
$C_{+2\sigma}$	0.0427	0.0346	0.0244
$(C_{+2\sigma} - C_{fit})/C_{fit}$	37.3%	37.8%	40.2%
δ	0.912	0.854	1.174

the whole set of experimental data. Considering specific propellant combinations, heat transfer dispersion with respect to the fit value is almost 50% in the case of oxygen–kerosene, almost 35% in the case of oxygen–hydrogen, and less than 30% in the case of oxygen–methane. In the case of oxygen–hydrogen, the dispersion reduces to about 20% if the heat transfer correlation includes geometric parameters like the throat radius of curvature, the convergence angle, and the contraction ratio while in the case of oxygen–kerosene the dispersion reduces to about 40% if the heat transfer correlation includes the oxidizer-to-fuel mass mixture ratio. The latter term is probably linked to the effect of a mild soot deposition at the wall. In conclusion, the proposed correlations and the associated data dispersion, hardly below 20%, indicate that a new thrust chamber can be designed using simplified and general rules only if sufficiently large design margins are taken into account. More accurate estimation of the heat transfer can be obtained only by testing the specific thrust chambers and injectors to be characterized. The use of the computational fluid-dynamics, provided that it is sufficiently accurate, can partially alleviate the effort of the experimental characterization.

Declaration of competing interest

The authors declare that they have no known competing financial interests or personal relationships that could have appeared to influence the work reported in this paper.

References

[1] J.L.B. Selwood, Some observations on the problems of rocket-motor cooling design, J. Am. Rocket Soc. (76) (1949) 16–26, http://dx.doi.org/10.2514/8.4256.

[2] R. Gordon, Heat-transfer problems in liquid-propellant rocket motors, J. Am. Rocket Soc. (81) (1950) 65–78, http://dx.doi.org/10.2514/8.4316.

[3] L.H. Back, P.F. Massier, H.L. Gier, Convective heat transfer in a convergent-divergent nozzle, Int. J. Heat Mass Transfer 7 (5) (1964) 549–568, http://dx.doi.org/10.1016/0017-9310(64)90052-3.

[4] D.R. Boldman, J.F. Schmidt, R.C. Ehlers, Effect of uncooled inlet length and nozzle convergence angle on the turbulent boundary layer and heat transfer in conical nozzles operating with air, J. Heat Transfer 89 (4) (1967) 341–350, http://dx.doi.org/10.1115/1.3614395.

[5] D.R. Bartz, A simple equation for rapid estimation of rocket nozzle convective heat transfer coefficients, J. Jet Propuls. 27 (1) (1957) 49–51, http://dx.doi.org/10.2514/8.12572.

[6] M. Frey, T. Aichner, J. Görgen, B. Ivancic, B. Kniesner, O. Knab, Modeling of rocket combustion devices, in: AIAA paper 2010-4329, 2010, http://dx.doi.org/10.2514/6.2010-4329.

[7] J. Song, B. Sun, Coupled numerical simulation of combustion and regenerative cooling in LOX/methane rocket engines, Appl. Therm. Eng. 106 (2016) 762–773, http://dx.doi.org/10.1016/j.applthermaleng.2016.05.130.

[8] B. Betti, D. Bianchi, F. Nasuti, E. Martelli, Chemical reaction effects on heat loads of CH_4/O_2 and H_2/O_2 rockets, AIAA J. 54 (5) (2016) 1693–1703, http://dx.doi.org/10.2514/1.J054606.

[9] G. Leccese, D. Bianchi, B. Betti, D. Lentini, F. Nasuti, Convective and radiative wall heat transfer in liquid rocket thrust chambers, J. Propul. Power 34 (2) (2018) 318–326, http://dx.doi.org/10.2514/1.B36589.

[10] Y. Daimon, H. Negishi, H. Kawashima, Conjugated combustion and heat transfer simulations of upper and lower main combustion chambers of LE-9 engine, in: AIAA paper 2019-4112, 2019, http://dx.doi.org/10.2514/6.2019-4112.

[11] Y. Jin, X. Xu, Q. Yang, S. Zhu, Numerical investigation of flame appearance and heat flux and in a deep-throttling variable thrust rocket engine, Aerosp. Sci. Technol. 88 (2019) 457–467, http://dx.doi.org/10.1016/j.ast.2019.03.042.

[12] J. Xu, P. Jin, R. Li, J. Wang, G. Cai, Effect of coaxial injector parameters on LOX/methane engines: A numerical analysis, Acta Astronaut. 171 (2020) 225–237, http://dx.doi.org/10.1016/j.actaastro.2020.02.055.

[13] C.E. Dexter, M.F. Fisher, J.R. Hulka, K.P. Denisov, A.A. Shibanov, A.F. Agarkov, Scaling techniques for design, development, and test, in: V. Yang, M. Habiballah, J. Hulka, M. Popp, Progress in Astronautics and Aeronautics, Vol. 200 (Eds.), Liquid Rocket Thrust Chambers: Aspects of Modeling, Analysis, and Design, AIAA, Washington, DC, 2004, pp. 553–600, http://dx.doi.org/10.2514/5.9781600866760.0553.0600.

[14] D. Preclik, D. Wiedmann, W. Oechslein, J. Kretschmer, Cryogenic rocket calorimeter chamber experiments and heat transfer simulations, in: AIAA paper 98-3440, 1998, http://dx.doi.org/10.2514/6.1998-3440.

[15] A. Kumakawa, M. Sasaki, K. Sato, H. Tamura, F. ONO, H. Sakamoto, N. Yatsuyanagi, Hot gas side heat transfer characteristics of LOX/H_2 and LOX/HC type propellants, Report NAL-TR-1062T, Japan Aerospace Exploration Agency, JAXA, 1990.

[16] M. Popp, G. Schmidt, Heat transfer investigations for high pressure rocket combustion chambers, in: AIAA paper 94-3102, 1994, http://dx.doi.org/10.2514/6.1994-3102.

[17] A. Fröhlich, M. Popp, G. Schmidt, D. Thelemann, Heat transfer characteristics of H_2/O_2-combustion chambers, in: AIAA paper 93-1826, 1993, http://dx.doi.org/10.2514/6.1993-1826.

[18] R.J. Quentmeyer, R.L. Schacht, Axial and circumferential variations of hot-gas-side heat-transfer rates in a hydrogen-oxygen rocket, Report NASA-TN-D-6396, National Aeronautics and Space Administration, NASA, 1971, contract 122-29.

[19] V.V.A.A., Hydrogen-oxygen auxiliary propulsion for the space shuttle. Volume i: High pressure thrusters, Report NASA-CR-120895, National Aeronautics and Space Administration, NASA, 1973, contract NAS3-14354.

[20] D. Haeseler, D. Preclik, Heat flux management and cooling techniques in rocket thrust chambers, in: Proceedings of the 4^{Th} International Symposium on Liquid Rocket Propulsion; Lampoldshausen, Germany; 13-15 March 2000, German Aerospace Center, DLR, 2000, pp. 1–25.

[21] D.R. Bartz, Turbulent boundary-layer heat transfer from rapidly accelerating flow of rocket combustion gases and of heated air, Adv. Heat Transf. 2 (1965) 1–108, http://dx.doi.org/10.1016/S0065-2717(08)70261-2.

[22] W.R. Wagner, M. Shoji, Advanced regenerative-cooling techniques for future space transportation systems, in: AIAA paper 75-1247, 1975, http://dx.doi.org/10.2514/6.1975-1247.

[23] V.V.A.A., STE Thrust chamber technology: Main injector technology program and nozzle advanced development program (ADP), Report NASA-CR-193919, National Aeronautics and Space Administration, NASA, 1993, contract NAS8-37490.

[24] E.R.G. Eckert, Survey on heat transfer at high speeds, (Report WADC TR 54 070) Wright Air Development Center, United States Air Force, 1954.
[25] R. Cook, G. Coffey, Space shuttle orbiter engine main combustion chamber cooling and life, in: AIAA paper 73-1310, 1973, http://dx.doi.org/10.2514/6.1973-1310.
[26] S. Gordon, B.J. McBride, Computer program for calculation of complex chemical equilibrium compositions and applications (I. Analysis), Report NASA RP-1311, National Aeronautics and Space Administration, NASA, 1994, contract RTOP 505-62-52.
[27] S. Gordon, B.J. McBride, Computer program for calculation of complex chemical equilibrium compositions and applications (II. Users manual and program description), Report NASA RP-1311, National Aeronautics and Space Administration, NASA, 1996, contract RTOP 505-62-52.
[28] L. Schoenman, P. Block, Laminar boundary-layer heat transfer in low-thrust rocket nozzles, J. Spacecr. Rockets 5 (9) (1968) 1082–1089, http://dx.doi.org/10.2514/3.29425.
[29] R. Hernandez, J.I. Ito, K.Y. Niiya, Carbon deposition model for oxygen-hydrocarbon combustion. Volume i, Report NASA-CR-179375, National Aeronautics and Space Administration, NASA, 1987, contract NAS8-34715.
[30] R.J. Quentmeyer, R.L. Schacht, W.L. Jones, Hot-gas-side heat transfer with and without film cooling on a simulated nuclear rocket thrust chamber using H_2-O_2, Report NASA-TN-D-6638, National Aeronautics and Space Administration, NASA, 1972, contract RTOP 112-29.
[31] D. Fulton, Investigation of thermal fatigue in non-tubular regeneratively cooled thrust chamber. Final report. Volume i, Report AFRPL-TR-73-10(I), Rocketdyne Division, Rockwell International, 1973, contract F04611-70-C-0014.
[32] W.H. Nurick, W.S. Hines, Experimental investigation of combustor effects on rocket thrust chamber performance, Report NASA-CR-134187, National Aeronautics and Space Administration, NASA, 1973, contract NASW-2106.
[33] A.T. Zachary, Advanced space engine preliminary design, Report NASA-CR-121236, National Aeronautics and Space Administration, NASA, 1973, contract NAS3-16751.
[34] R.L. Ewen, C.J. Obrien, L.W. Matthews, Dual-throat thruster thermal model, Report NASA-CR-178975, National Aeronautics and Space Administration, NASA, 1986, contract NAS8-34136.
[35] J. Schneider, W.R. Hayden, Orbital transfer vehicle 3000 LBF thrust chamber assembly hot fire test program, Report NASA-CR-182145, National Aeronautics and Space Administration, NASA, 1988, contract NAS3-23772.
[36] S.K. Elam, Subscale LOX/hydrogen testing with a modular chamber and a swirl coaxial injector, in: AIAA paper 91-1874, 1991, http://dx.doi.org/10.2514/6.1991-1874.
[37] R.J. Quentmeyer, E.A. Roncace, Hot-gas-side heat transfer characteristics of subscale, plug-nozzle rocket calorimeter chamber, Report NASA-TP-3380, National Aeronautics and Space Administration, NASA, 1993, contract RTOP 584-03-11.
[38] M. Niino, A. Kumakawa, N. Yatuyanagi, H. Gomi, A. Suzuki, H. Sakamoto, M. Sasaki, K. Yanagawa, A study on heat transfer characteristics of water cooled LO_2/LH_2 rocket combustor, Report NAL-TR-708, Japan Aerospace Exploration Agency, JAXA, 1982, in Japanese.
[39] T. Haarmann, Numerische simulation des wärmeübergangs in einer kryogenen raketenbrennkammer (Ph.D. thesis), RWTH Aachen, Aachen, DE, 2006.
[40] R.J. LaBotz, D.C. Rousar, H.W. Valler, High-density fuel combustion and cooling investigation, Report NASA-CR-165177, National Aeronautics and Space Administration, NASA, 1980, contract NAS3-21030.
[41] C.R. Bailey, Oxygen/hydrocarbon combustion devices technology, in: Proceedings of the 1985 JANNAF Propulsion Meeting; San Diego,CA, USA; 9-12 April 1985, vol. I, The Johns Hopkins University, Applied Physics Laboratory, 1985, pp. 271–280.
[42] R. Hernandez, J.I. Ito, K.Y. Niiya, Carbon deposition model for oxygen-hydrocarbon combustion. Vol. II, Report NASA-CR-179376, National Aeronautics and Space Administration, NASA, 1987, contract NAS8-34715.
[43] P.A. Masters, E.S. Armstrong, H.G. Price, High-pressure calorimeter chamber tests for liquid oxygen/kerosene (LOX/RP-1) rocket combustion, Report NASA-TP-2862, National Aeronautics and Space Administration, NASA, 1988, contract RTOP 582-01-11.
[44] J. Volkmann, L. Tuegel, J. McLeod, Gas side heat flux and film coolant investigation for advanced LOX/hydrocarbon thrust chambers, in: AIAA paper 90-2184, 1990, http://dx.doi.org/10.2514/6.1990-2184.
[45] H.A. Arbit, L.M. Tuegel, F.E. Dodd, Heavy hydrocarbon main injector technology program, Report NASA-CR-184161, National Aeronautics and Space Administration, NASA, 1991, contract NAS8-36369.
[46] L.R. May, W.M. Burkhardt, Transpiration cooled throat for hydrocarbon rocket engines, Report NASA-CR-184272, National Aeronautics and Space Administration, NASA, 1991, contract NAS8-36952.
[47] J.G. Kim, K.J. Lee, S. Seo, Y.M. Han, H.J. Kim, H.S. Choi, Film cooling effects on wall heat flux of a liquid propellant combustion chamber, in: AIAA paper 2006-5196, 2006, http://dx.doi.org/10.2514/6.2006-5196.
[48] G.M. Meagher, J.A. Muss, Swirl coaxial injector element characterization for booster engines, in: Advanced Earth-To-Orbit Propulsion Technology 1988, vol. 1, National Aeronautics and Space Administration, NASA, 1988, pp. 334–347.
[49] R.J. Jensen, H.C. Dodson, S.E. Claflin, LOX/Hydrocarbon combustion instability investigation, Report NASA-CR-182249, National Aeronautics and Space Administration, NASA, 1989, contract NAS3-24612.
[50] V.V.A.A., Combustion performance and heat transfer characterization of LOX/Hydrocarbon type propellants. Task II: Data dump, Report NASA-CR-171629, National Aeronautics and Space Administration, NASA, 1983, contract NAS9-15958.
[51] C.H. Liebert, R.C. Ehlers, Determination of local experimental heat-transfer coefficients on combustion side of an ammonia-oxygen rocket, Report NASA-TN-D-1048, National Aeronautics and Space Administration, NASA, 1961.
[52] R.K. Rose, Experimental determination of the heat flux distribution in a rocket nozzle, Report F-58-1, Purdue University, 1958, contract N7 onr 39418.
[53] A.B. Witte, E.Y. Harper, Propulsion division; xII. Liquid propellant propulsion; b. Heat transfer and fluid mechanics, Report Research Summary No. 36-10. Volume I, Jet Propulsion Laboratory, JPL, 1961, pp. 87–91.
[54] W.E. Welsh Jr., A.B. Witte, A comparison of analytical and experimental local heat fluxes in liquid-propellant rocket thrust chambers, J. Heat Transfer 84 (1) (1962) 19–28, http://dx.doi.org/10.1115/1.3684282.
[55] A.B. Witte, E.Y. Harper, Experimental investigation of heat transfer rates in rocket thrust chambers, AIAA J. 1 (2) (1963) 443–451, http://dx.doi.org/10.2514/3.1552.
[56] W.A. Carter, G.S. Bell, Development and demonstration of a N_2O_4-N_2H_4 injector, Report AFRPL-TR-69-231, Air Force Rocket Propulsion Laboratory, 1969.
[57] R.P. Pauckert, Space storable regenerative cooling investigation. Final report, Report NASA-CR-72705, National Aeronautics and Space Administration, NASA, 1970, contract NAS3-11191.
[58] S.D. Clapp, A.Y. Falk, C.K. Nagai, Space storable propellant performance study. Final report, Report NASA-CR-72487, National Aeronautics and Space Administration, NASA, 1968, contract NAS3-11199.
[59] H.A. Arbit, S.D. Clapp, C.K. Nagai, Lithium-fluorine-hydrogen propellant investigation. Final report, Report NASA-CR-72695, National Aeronautics and Space Administration, NASA, 1970, contract NAS3-11230.
[60] L.H. Back, H.L. Gier, P.F. Massier, Convective heat transfer in a convergent-divergent nozzle, Report NASA-CR-57326, National Aeronautics and Space Administration, NASA, 1965, contract NAS7-100.
[61] D.R. Boldman, H.E. Neumann, J.F. Schmidt, Heat transfer in 30 deg and 60 deg half-angle of convergence nozzles with various diameter uncooled pipe inlets, Report NASA-TN-D-4177, National Aeronautics and Space Administration, NASA, 1967, contract 129-01-09-06-22.
[62] D.R. Boldman, R.W. Graham, Heat transfer and boundary layer in conical nozzles, Report NASA-TN-D-6594, National Aeronautics and Space Administration, NASA, 1972, contract RTOP 132-15.
[63] J.W. Magee, T.J. Bruno, D.G. Friend, M.L. Huber, A. Laesecke, E.W. Lemmon, M.O. McLinden, R.A. Perkins, J. Baranski, J.A. Widegren, Thermophysical properties measurements and models for rocket propellant RP-1: Phase i, Report NISTIR 6646, National Institute of Standards and Technology, NIST, 2007.